Protein Mechanics

Onck, Patrick

Published in:
Procedia IUTAM

DOI:
10.1016/j.piutam.2017.03.010

Publication date:
2017

Available online at www.sciencedirect.com

ScienceDirect

Procedia IUTAM 20 (2017) 73 – 80

Procedia IUTAM

www.elsevier.com/locate/procedia

XXIV ICTAM, 21-26 August 2016, Montreal, Canada

PROTEIN MECHANICS: FROM AMINO ACID TO SWIMMING CELLS

Patrick Onck

Micromechanics, Zernike Institute for Advanced Materials, University of Groningen, Groningen, The Netherlands

Abstract

This proceedings paper contains a review of the work presented in the Sectional Lecture in Solids on August 25 at ICTAM 2016. -- Proteins are long polypeptide chains of amino acids and their structure and biological function are directly related to their amino acid sequence. I will discuss three different biological functions that are dominated by protein mechanics, each at their own specific time and length scale. To relate structure to function, multiscale computational models have been developed for (i) cilia and flagella, (ii) actin filament networks and (iii) the nuclear pore complex.

Peer-review under responsibility of organizing committee of the 24th International Congress of Theoretical and Applied Mechanics

Keywords: proteins; computational biomechanics; biophysics; molecular dynamics, actin networks, nuclear pore complex, cilia and flagella.

1. Introduction: Proteins

Proteins are often referred to as the building blocks of life, playing critical roles in almost all structures and activities in biology. Fig. 1 provides an overview of the different length scales of proteins discussed in this review, starting from the atomic scale and ending at the scale of cells. At the smallest, atomic length scale, proteins consist of amino acids. There are 20 different amino acids, each with their own atomic structure, chemical and physical properties. The amino acids form peptide bonds that form long polypeptide chains consisting of hundreds and sometimes thousands of amino acids. Depending on the specific amino-acid sequence (primary structure) the polypeptide chains fold into regular structures, such as α-helices and β-sheets (secondary structure). At a larger spatial level of organization, α-helices and β-sheets will fold into three-dimensional (tertiary) structures, i.e., the actual protein molecule. Finally, protein molecules can combine to form large protein complexes (quaternary structures). In this Proceedings paper I will discuss three different quaternary structures: (i) cilia and flagella in section 2.1, (ii) actin filament networks in section 2.2 and (iii) the nuclear pore complex (NPC) in section 2.3.

Peer-review under responsibility of organizing committee of the 24th International Congress of Theoretical and Applied Mechanics
doi:10.1016/j.piutam.2017.03.010

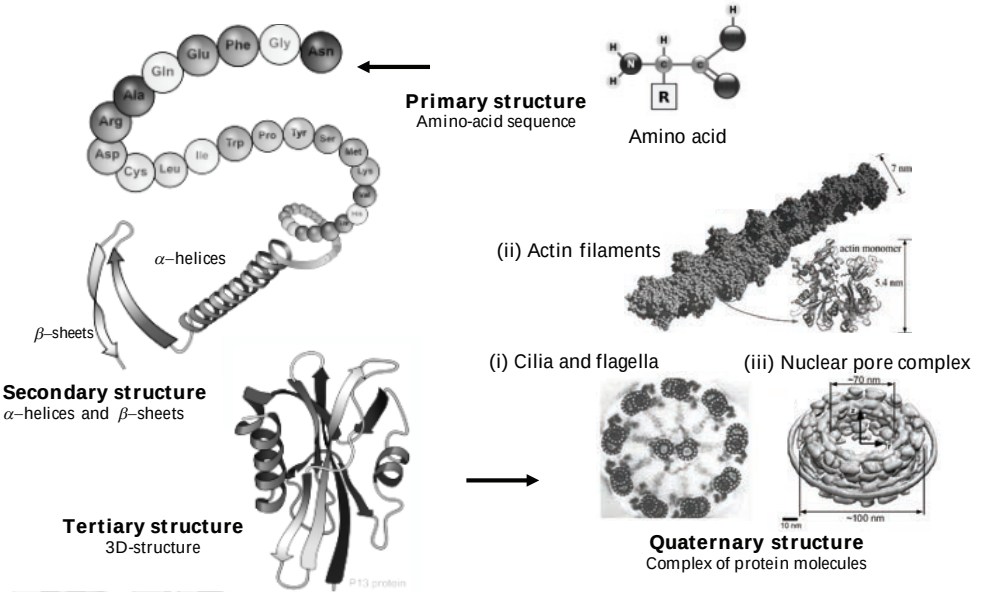

Fig. 1. Overview of the different length scales of proteins. Proteins consist of long polypeptide chains consisting of hundreds of amino-acids. The amino-acids is the smallest building block of proteins, consisting of 10 atoms on average. These amino-acid sequences form the primary structure of proteins. Depending on the specific amino-acid sequence the polypeptide chains fold into ordered structures: α-helices and β-sheets, the secondary structure of proteins. At an even larger spatial level the secondary structures combine into the three-dimensional (tertiary) structure, often referred to as the actual protein molecule or subunit. Finally, the protein molecules can combine into large protein complexes (quaternary structures), such as actin filaments, cilia and flagella, and the nuclear pore complex (NPC). Image sources: [1-4].

2.1 Cilia and flagella

At the largest length scale, we focus on cilia and flagella, long hair-like projections from the surface of cells that play an important role in cell motility [5], see Fig. 2. Cells and micro-organisms use cilia and flagella to propel themselves or to propel the fluid surrounding them. Examples are the beating tails (flagella) of sperm cells (see Fig. 2c), or the cilia that line the respiratory tract to propel mucus out of the lungs. The beating of cilia and flagella is enabled by their internal microstrucure, the axoneme (see Fig. 2b), a big protein complex (tens of μm long and 250 nm wide) that is powered by a dense distribution of motor proteins, called dyneins (Fig. 2a). Motor proteins constitute an important class of proteins that, powered by the hydrolysis of ATP, undergo

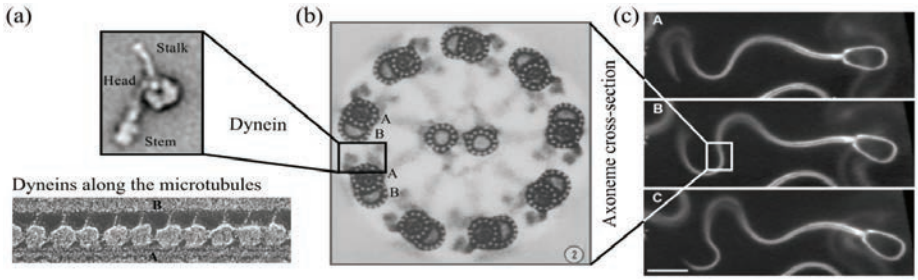

Fig. 2.: (a) Structure of an axonemal dynein (top). Dyneins at a regular spacing along the microtubules (bottom) (from [6]). (b) An electron micrograph of an axoneme cross-section (from [7]). (c) Flagellar beating of a spermatozoon. The three images (A-C) are 200 ms apart (from[8]). The total figure appeared before in [9].

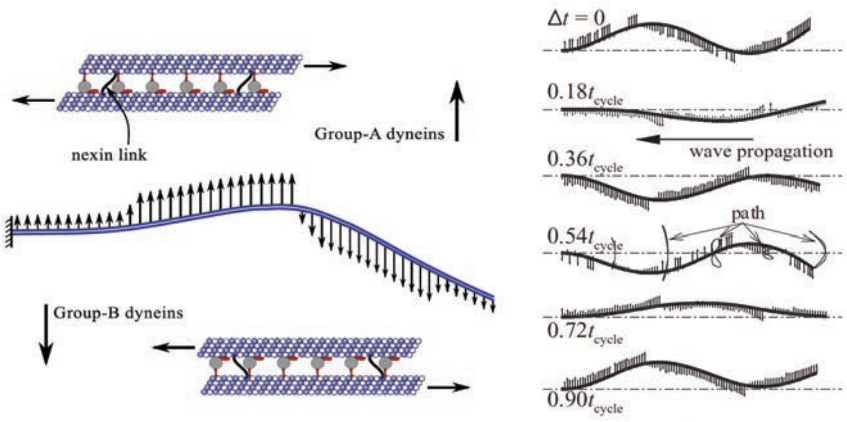

Fig 3: (a) A representative computational model of the axoneme structure where two microtubules are connected via nexin links. Two groups (A and B) of dyneins are present at a regular spacing along the microtubules, each responsible for sliding in opposite directions. The dynein activity is shown by the vertical arrows, where the length of an arrow indicates the magnitude of the respective dynein force. Note that the actual dynein force is tangential to the axoneme (from [9]). (b) The dynein activity along the axonemal length with time is shown by the vertical arrows indicating the dynein coordination (temporal as well as spatial) causing an evolution of local bend regimes in the microtubules and their propagation with time (from [9]).

conformational changes and as such convert chemical energy into mechanical work. We developed a computational model based on a minimal representation of the axoneme (see Fig. 3a) to study planar beating of natural flagella due to the coordinated operation of ATP-powered dyneins [9]. The axoneme structure is modeled by two representative (doublet) microtubules that are connected via nexin links. We analyze this system using a two-dimensional computational model in which an integral formulation for Stokes flow is implemented using the boundary element method to represent the fluid environment, while the microtubules and nexin links are represented by beam elements. The solid mechanics and fluid dynamics equations are implicitly coupled, details of which can be found in [9,10]. We account for two groups of dyneins (groups A and B), each responsible for sliding (of the neighboring microtubules) in opposite directions; see Fig. 3(a). The dynein activity is shown by the vertical arrows, where the length of an arrow indicates the magnitude of the applied dynein force. We assume that all the dyneins are the same and are placed with a constant spacing. We postulate a “negative-work-based deactivation” of the dyneins, which prompts an active dynein to go into an inactive state at the occurrence of sliding in the negative direction (i.e., opposite to its “natural” sliding direction). In addition, we employ a time delay in the physical switching mechanism, which has often been reported in the literature [11,12]. The axoneme deformation and dynein activity are shown in Fig. 3b. We observe an emergence of dynein coordination (temporal as well as spatial) causing an evolution of local bend regimes in the axoneme and their propagation with time. The regular beating spontaneously emerges as a result of the switching mechanism (a time delayed deactivation of the dyneins based on negative work), imposed on an initially planar configuration of the axoneme with a spatially random distribution of (initial) dynein activity.

From a biotechnology point of view, the beating of cilia and flagella are interesting examples for bio-mimicry, utilizing millions of years of biological evolution that led to optimized biological actuators at low Reynolds numbers. Here, artificial, bio-inspired cilia and flagella can be designed using light [13] or magnetic [14-17] actuation to mimic the non-reciprocal motion of their biological counter-part. Artificial cilia can effectively propel fluids in lab-on-chip microfluidic systems, resolving the scale-related problems of downsizing conventional pumping systems [18,19].

2.2 Actin filament networks

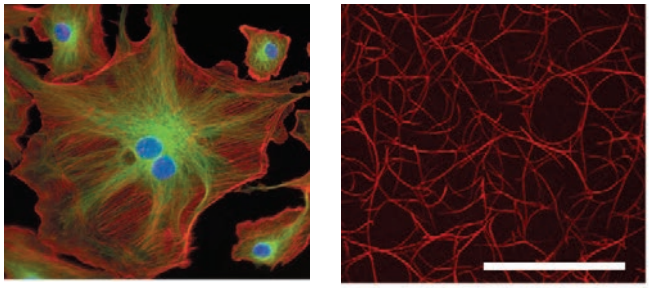

Fig. 4: (left) Endothelial cells attached to a substrate, depicting the actin cytoskeleton (red), microtubuli (green) and the nucleus (blue) (from [20]). (right) Cross-linked actin filament networks (from [21]).

At a somewhat smaller, subcellular length scale, living cells contain networks of cytoskeletal proteins (Fig. 4). The cytoskeleton is the key cellular component that is responsible for the mechanical behavior of the cell. The major cytoskeletal network is formed by the protein actin, which assembles into a filamentous quaternary structure, and is responsible for maintaining cell shape, stability and for cell motility. Depending on the function and location in the cell, the actin network is cross-linked by different cross-binding proteins, each with their own molecular structure. To capture the constitutive response of actin and other protein networks, we developed a discrete computational network model in two and three dimensions to study the strain stiffening of cross-linked protein networks at large strains [22-24]. Here I review the three-dimensional simulations that appeared in [24] and [25].

We use a numerical method to self-assemble a fully periodic representative volume element (RVE) of an athermal, random fibre network in three dimensions, see Fig. (5a) [26]. This network generation procedure simulates the fibre dynamics subject to a weak attractive force field between fibres such that a homogeneous, isotropic random network assembles. The fibres are subsequently discretized by beam elements and implemented into a nonlinear finite-element code with axial, torsional and bending properties that mimic semiflexible biopolymers, such as actin, tubulin, fibrin and collagen. A range of different networks are generated with different fibre architectures, characterized by different fibre-lengths l_0, cross-link distances l_c (the average distance between the crosslinks, shown in red in Fig. 5(a)) and filament concentrations c_f. The networks are subjected to shear strains Γ and the shear stress T is recorded, giving, upon differentiation, the shear stiffness G as a function of shear stress T (See Fig. 5(b)). The inset shows that at small stresses the stiffness is equal to the small strain stiffness G_0, which is dominated by bending. Then, at a certain critical stress T_C, the network response becomes highly non-linear, transiting from a bending dominated to a more stretching dominated response. In the stiffening regime of the curves, the shear stiffness scales with $T^{3/2}$, as observed in many rheological experiments on different cross-linked fibre networks that are polymerized in-vitro. Upon normalizing the stresses by the critical stress all results collapse into a unique master curve (Fig. 5(b)). We carefully inspected the critical strain Γ_C (related to the critical stress through $\Gamma_C = T_C / G_0$) and found that this can be captured by a

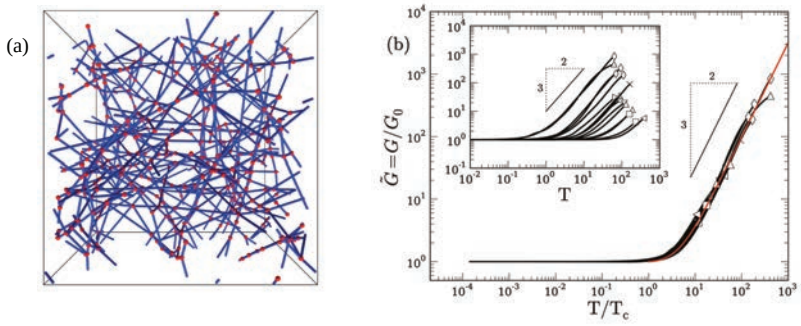

Fig. 5. (a) The cross-linked actin network model. The image shows of a generated RVE with actin fibers shown in blue and cross-links in red. The RVE is loaded in shear with periodic boundary conditions (from [24]). (b) After scaling the network modulus G by G_0 and stress T by the critical stress T_c all data (inset) collapse onto a master curve (from [25]).

unique relation that depends solely on the topological parameter defined as the ratio between filament length and cross-link distance l_0 / l_c. The resulting master curve thus fully captures the response of a wide range of different cross-linked networks with largely differing architectures, whose large-strain stress-strain response can be uniquely determined once the small strain stiffness is known in addition to the topological parameter l_0 / l_c.

2.3 The nuclear pore complex (NPC)

It has long been thought, that proteins need to have a folded structure to perform their function (see Fig. 1), but more and more evidence is appearing that suggests that also natively unfolded proteins play an important role in many biological processes. One of these roles is in controlling the transport of proteins and nucleic acids in and out of the nucleus of living cells. This transport is mediated by a very large quaternary protein structure, the nuclear pore complex (NPC), see Fig. 1. Multiple NPCs are embedded in the membrane of the cell nucleus (see Fig. 6(a)) and feature a structure that consists of 30 different proteins, called nucleoporins (nups). A considerable part of these nups (approximately 20) are folded proteins that anchor the NPC inside the nuclear membrane and form a ring scaffold (see Fig. 6(b)). However, the remaining (approximately) 10 nups are natively unfolded proteins, i.e., they have an amino-acid sequence that is such that no stable secondary structures are formed (see Fig. 1). These natively-unfolded nups (called FG-nups because they are rich in the amino-acids phenylalanine (F) and glycine (G)) are anchored at the inner surface of the pore scaffold at specific locations. The FG-nups are key in controlling transport, but how they exactly do that is as of yet unknown. This is the goal of the current investigation.

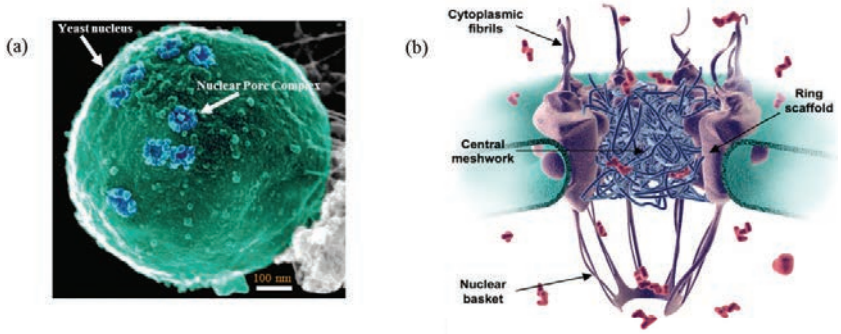

Fig. 6. (a) Nucleus of a yeast cell (green). Embedded in the nuclear membrane are nuclear pore complexes (blue), large protein complexes that mediate transport in and out of the nucleus (from [27]). (b) Schematic of the nuclear pore complex. The blue central region highlights the natively unfolded FG-Nups that are held responsible for the remarkable selectivity of protein transport across the pore. The scale from top to bottom is about 100 nm (from [28]).

Yeast NPCs have approximately 160 FG-nups, each FG-nup contains around 800 amino-acids and each amino-acid has approximately 10 atoms, resulting in 1.3 million protein atoms. This many atoms, together with the even larger amount of atoms in the water molecules, makes this a formidable task for atomistic calculations. We therefore developed a coarse-grained approach in which each amino-acid is represented by one bead and in which the water is only implicitly accounted for through coarse-grained potentials and Langevin dynamics [29-32]. This one-bead-per-amino-acid (1BPA) molecular dynamics model distinguishes between all 20 amino acids of the nups and takes into account hydrophobic and electrostatic interactions. We built a simplified version of the nuclear pore complex (see Fig. 7(a)) and anchored the FG-nups inside the pore according to experimentally-found discrete anchor locations (see Fig. 7(b)). Fig. 7(c) shows the time-averaged density distribution of the amino-acids inside the NPC showing that the nups collectively form a high-density, doughnut-like ring [30].

Because the distribution of the FG-nups is relatively homogeneous in the circumferential direction, it can be averaged to generate a two-dimensional, r –z density map (see Fig. 8(a), wild-type-1). A second simulation (wild-type-2) with the same FG-nups but different starting configuration and initial velocity distribution is performed,

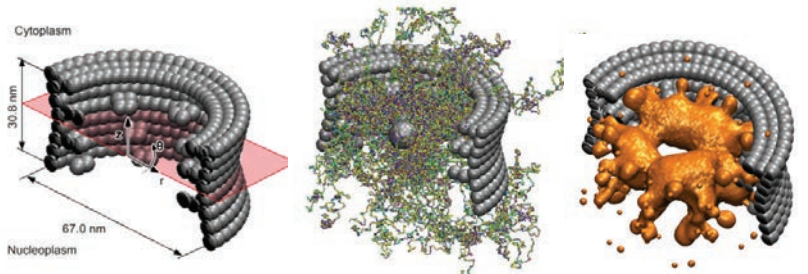

Fig. 7. (a) Structural model of the NPC featuring a rigid scaffold constructed by 5 nm-sized rigid beads. (b) All natively unfolded (FG-) nups are tethered to the scaffold at their anchor point locations. Figs. (a) and (b) are taken from [32]. (c) Time-averaged density distribution showing a doughnut-like amino-acid density distribution (from [30]).

showing the same characteristics as that of the first simulation (Fig. 8(b)). To investigate the contribution of the hydrophobic and electrostatic interactions to the donut-shape, we removed the charged residues and replacing them with neutral beads. The resulting density plot of this no-charge NPC shows that all FG-nups aggregate in a wide, high-density region (Fig. 8(c)). In a next step, the rest of the amino acids are also replaced with neutral beads, resulting in a so-called 'denatured' NPC, showing a uniform distribution of low density throughout the pore (Fig. 8(d)). The results indicate that repulsive interactions between the charged amino acids in the wild-type NPC serve as a bumper to push the dense FG-nup clusters, formed through hydrophobic interactions, toward the center of the pore. Therefore, the doughnut-like structure in Fig. 7(c) is a direct result of the balance between the electrostatic and hydrophobic interactions. Next, we explore the effect of the FG-nup amino acid sequence on the density distribution in the wild-type NPC. To do so, we simply turned around the FG-nups by tethering them at their N-terminus instead of C-terminus to the same anchoring points. The distribution for this reversed NPC is shown in Fig. 8(e). Finally, a uniform NPC is simulated where the residues in the sequence of the FG-nups are reshuffled such that the charged and hydrophobic amino acids become uniformly distributed along their length (Fig. 8(f)). The density distributions for both the reversed and uniform NPC are different from the wild-type NPC. In these two cases, the amino-acid composition of the FG-nups (percentage of charged and hydrophobic amino acids) has not changed compared to the wild-type NPC, suggesting that the amino-acid sequence of the FG-nups plays a key role in the density distribution of the FG-nups in the wild-type NPC.

References

[1] Sataric MV, Sekulic DL and Sataric BM 2015 Actin filaments as the fast pathways for calcium ions involved in auditory processes. J. Biosci. 40 549–559]
[2] https://en.wikipedia.org/wiki/Protein, https://en.wikipedia.org/wiki/Amino_acid.
[3] Alber, F., Dokudovskaya, S., Veenhoff, L., Zhang, W., Kipper, J., Devos, D., Suprapto, A., Karni- Schmidt, O., Williams, R., Chait, B. et al.: 2007, The molecular architecture of the nuclear pore complex, Nature 450(7170), 695–701.
[4] Bruce Alberts, Alexander Johnson, Julian Lewis, David Morgan, Martin Raff, Keith Roberts, Peter, Molecular Biology of the Cell, 6th Edition, ISBN: 9780815344322 (2014).
[5] M.A. Sleigh, Cilia and flagella. Academic Press, London, New York, (1974).
[6] Goodenough and Heuser, J. Cell Biol. 95, 798–815 (1982).
[7] Afzelius et al., Tissue and Cell 27, 241–247 (1995)].
[8] Woolley et al., *J. Exp. Biol.* 212, 18
[9] S.N. Namdeo and P.R. Onck, The emergence of flagellar beating from the collective behavior of individual ATP-powered dyneins, Physical Review E. 94, 4, 15 p., 042406
[10] S.N. Khaderi and P.R. Onck (2012). Fluid-structure interaction of three-dimensional magnetic artificial cilia, *J. Fluid Mech*. 708, 303-328.
[11] T. Guerin, J. Prost, and J.-F. Joanny, Dynamical behavior of molecular motor assemblies in the rigid and crossbridge models, Eur. Phys. J. E 34, 1 (2011).

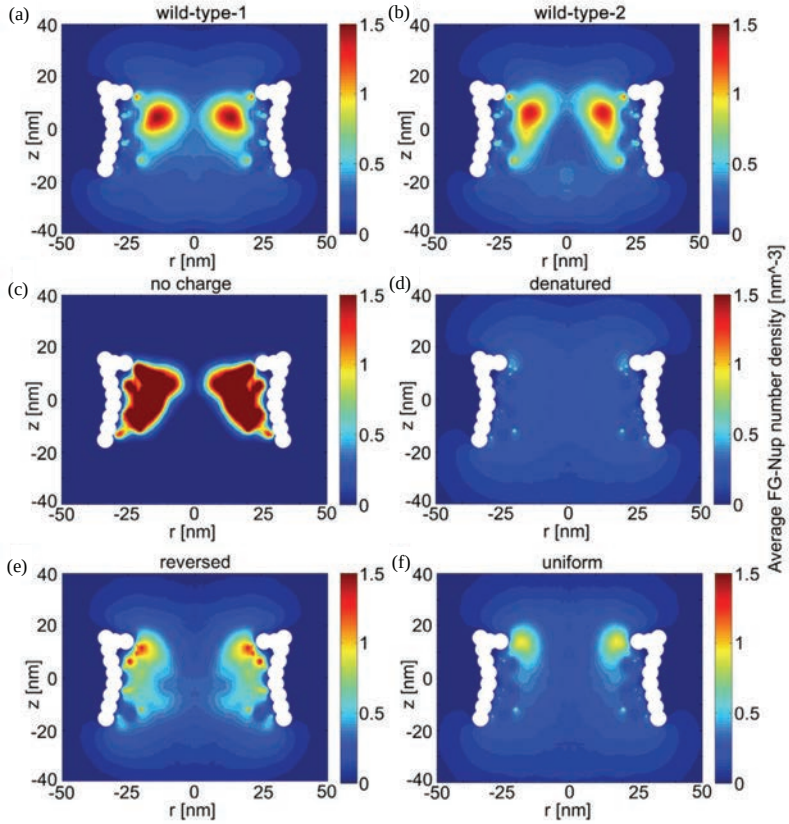

Fig. 8. (a) Tw-dimensional (r-z) density plots of the FG-nups in the simulated NPCs. (a) Wild-type-1NPC. (b) Wild-type-2 NPC, simulated with a different starting configuration and initial velocity distribution compared to wild-type-1. (c) No-charge NPC, in which all charged residues are replaced by neutral beads in the sequence of the FG-nups. (d) Denatured NPC, where all residues are replaced by neutral beads. (e) Reversed NPC, where the the FG-nups are anchored from their N-terminus. (f) Uniform distribution of charged and hydrophobic amino acids.

[12] D. Oriola, H. Gadelha, C. Blanch-Mercader, and J. Cas ade- munt, Subharmonic oscillations of collective molecular motors, Europhys. Lett. 107, 18002 (2014).
[13] D. Liu, L. Liu, P.R. Onck* and D.J. Broer*, Reverse switching of surface roughness in a self-organized polydomain liquid crystal coating. *P. Natl. Acad. Sci. USA* **112**:3880-3885 (2015). *Corresponding authors
[14] S.N. Khaderi, J.M.J. den Toonder and P.R. Onck, Magnetic artificial cilia for microfluidic propulsion. *Adv. Appl. Mech.* 48, 1-78 (2015).
[15] S.K. Namdeo, S.N. Khaderi and P.R. Onck, Numerical modeling of chirality-induced bi-directional swimming of artificial flagella *Proc. Royal Soc.* A 470 0130547 (2014)
[16] S.N. Khaderi and P.R. Onck (2012). Fluid-structure interaction of three-dimensional magnetic artificial cilia, *J. Fluid Mech*. 708, 303-328.
[17] S. N. Khaderi, C. B. Craus, J. Hussong, N. Schorr, J. Belardi, J. Westerweel, O. Prucker, J. Ruhe, J.M.J. den Toonder and P. R. Onck, Magnetically-actuated artificial cilia for microfluidic propulsion. *Lab Chip* 11, 2002–2010 (2011)
[18] J.M.J. den Toonder and P.R. Onck, Microfluidic manipulation with artificial/bioinspired cilia, *Trends Biotechnol.* 31, 85−91 (2013).
[19] J.M.J. den Toonder and P.R. Onck, P.R. (Eds.) *Artificial cilia*. Cambridge, RSC Publishing (2013).
[20] http://probes.invitrogen.com (date consulted: December 12, 2016).
[21] Schmoeller et al., *Biophys. J.* 97, 83–89 (2009).
[22] P.R. Onck, T. Koeman, T. van Dillen, E. Van der Giessen, An alternative explanation of stiffening in cross-linked semiflexible networks, *Phys. Rev. Lett*. 95 (17), 178102 (2005).

[23] T. van Dillen, P.R. Onck and E. Van der Giessen, Models for stiffening in cross-linked biopolymer networks: A comparative study, *J. Mech. Phys. Solids* 56 (2008) 2240–2264.
[24] G. Zagar, P.R. Onck, E. Van der Giessen, Two fundamental mechanisms govern the stiffening of cross-linked networks. *Biophys. J.* 108, 1470-1479 (2015).
[25] G. Zagar, P.R. Onck, E. Van der Giessen (2011). Elasticity of Rigidly Cross-Linked Networks of Athermal Filaments. *Macromolecules, 44*(17), 7026-7033.
[26] Huisman, E. M., T. van Dillen, ., E. Van der Giessen (2007). Three-dimensional cross-linked F-actin networks: relation between network architecture and mechanical behavior. Phys. Rev. Lett. 99:208103.
[27] Kiseleva, Nat. Cell. Biol. 6, 497, (2004).
[28] S. Patel, B. J. Belmont, J. M. Sante, and M. F. Rexach, Cell 129, 83 (2007).
[29] A. Ghavami, E. Van der Giessen and P.R.Onck, Coarse-grained potentials for local interactions in unfolded proteins, *J. Chem. Theory Comp.* 9 432−440 (2013).
[30] A. Ghavami, L.M. Veenhoff, E. Van der Giessen and P.R.Onck, Probing the disordered domain of the nuclear pore complex through coarse-grained molecular dynamics simulations, *Biophys. J.* 107, 1393–1402 (2014).
[31] P. Popken, A. Ghavami, P.R. Onck, B. Poolman and L.M. Veenhoff, Size-dependent leak of soluble and membrane proteins through the yeast nuclear pore complex. *Mol. Biol. Cell*, 26(7), 1386-1394 (2015).
[32] Ghavami, A., van der Giessen, E., and Onck, P. R. (2016). Energetics of Transport through the Nuclear Pore Complex. PLoS ONE, 11(2), 1-13. [e0148876].